

Physical Implications of *RHESSI* Neutron Capture-Line Measurements

R. J. Murphy and G. H. Share

E.O. Hulburt Center for Space Research, Code 7650, Naval Research Lab., Washington, DC 20375, U.S.A.

X.-M. Hua

L3 Communications, EER Systems, Inc., Largo, MD 20774, U.S.A

Robert P. Lin and David M. Smith

Space Sciences Laboratory and Dep't. of Physics, University of California, Berkeley, CA 94720, U.S.A.

Richard A. Schwartz

NASA Goddard Space Flight Center, Greenbelt, MD 20771, U.S.A.

ronald.murphy@nrl.navy.mil, gerald.share@nrl.navy.mil,
xinminh@gsfcsr4.gsfcmo.ecs.nasa.gov, rlin@ssl.berkeley.edu,
dsmith@taiyan.ssl.berkeley.edu, richard.schwartz@gsfcmo.nasa.gov

ABSTRACT

We report high spectral-resolution measurements of the 2.223 MeV neutron capture-line obtained with the *Reuven Ramaty High Energy Spectroscopic Imager* from the 2002 July 23 solar flare. The time history of this line is affected by both the photospheric ^3He abundance and the angular distribution of the interacting flare-accelerated particles producing the neutrons. The measured time history is compared with predicted time histories calculated using a magnetic loop model with a magnetic field perpendicular to the solar surface at the footpoints. The model includes energy losses due to Coulomb collisions, removal by nuclear reactions, magnetic mirroring in the convergent flux tube, and MHD pitch-angle scattering in the corona. This is the first analysis of the neutron-capture line using such a physically-based model. The derived constraints on the interacting angular distribution require that the accelerated particles had to suffer pitch-angle scattering during their transport through the coronal portion of the loop. The derived photospheric $^3\text{He}/\text{H}$ ratio was not well-constrained, primarily due to uncertainties associated with the measured nuclear deexcitation-line flux used to represent the neutron-production time profile.

Subject headings: Sun: abundances — Sun: flares — Sun: X-rays, gamma rays
 — nuclear reactions — acceleration of particles — turbulence

1. Introduction

The *Reuven Ramaty High Energy Spectroscopic Imager (RHESSI)* detected the 2.223 MeV neutron capture-line from the 2002 July 23 solar flare. Because the line is very narrow (<100 eV), the *RHESSI* high-resolution Ge detectors are very effective for observing it. The only previous high-resolution detection was by HEAO 3 from the 1979 November 9 flare (Prince et al. 1982) but analysis of those data was limited by the low counting rate. The line is formed when flare-produced neutrons are captured on ambient hydrogen in the photosphere producing deuterium. Since the neutrons slow down before capture, the line is delayed by ~ 100 s. The delay is affected by both the photospheric ${}^3\text{He}$ abundance and the angular distribution of the interacting particles producing the neutrons. Neutron capture on ${}^3\text{He}$, ${}^3\text{He}(n,p){}^3\text{H}$, produces no radiation but shortens the delay of the capture line (Wang & Ramaty 1974). Downward-directed interacting accelerated particles tend to produce neutrons deeper in the atmosphere where the higher density also shortens the delay.

Several investigators have determined the photospheric ${}^3\text{He}/\text{H}$ ratio using capture-line time-history measurements obtained with *SMM*, *GRANAT* and *CGRO*. Chupp et al. (1981); Prince et al. (1983); Trotter et al. (1993); Murphy et al. (1997) and Rank et al. (2001) approximated the expected line time history from instantaneous neutron production as the sum of exponentials and made simplifying assumptions about the density structure of the solar atmosphere and the interacting-particle angular distribution. Hua & Lingenfelter (1987b) used a Monte Carlo technique to calculate the depth, energy, and angular distribution of neutron and neutron capture-line production. The derived ${}^3\text{He}/\text{H}$ ratios from these analyses ranged from 0 to 5×10^{-5} , with the smallest uncertainties ($1\text{--}2 \times 10^{-5}$) obtained by Hua & Lingenfelter (1987b) and Rank et al. (2001). In these latter two analyses, the ${}^3\text{He}/\text{H}$ uncertainty was determined with a fixed interacting-particle angular distribution and without considering the uncertainties of the measured time history used to represent the neutron-production time profile. As a result, the ${}^3\text{He}/\text{H}$ uncertainties were underestimated.

In this paper we will use *RHESSI* observations of the neutron-capture line to determine the photospheric ${}^3\text{He}$ abundance. We will simultaneously vary both ${}^3\text{He}/\text{H}$ and the interacting-particle angular distribution and will include the effect of uncertainties of the neutron-production time profile. This will result in more realistic uncertainty estimates. Neutron capture-line time histories will be calculated using a magnetic loop model with a magnetic field perpendicular to the solar surface at the footpoints. The interacting-particle

angular distribution will be parameterized by the level of pitch-angle scattering (PAS) present in the loop which directly affects the distribution. The analysis will therefore also place constraints on the level of this scattering. We discuss the calculations and the loop model in §2 and present the data and compare them with the calculations in §3.

2. Neutron Capture-Line Calculations

Neutron capture-line production is very sensitive to the interacting accelerated-particle angular distribution. In previous analyses of neutron-capture line data, various analytic shapes for this distribution were assumed. Here, we use a physically-based magnetic loop model (Hua et al. 1989, 2002) to calculate the distribution. The model consists of a semi-circular coronal portion and two straight portions extending vertically from the transition region into the photosphere. Below the transition region, the magnetic field strength is assumed proportional to a power δ of the pressure (Zweibel & Haber 1983). The atmospheric model above 120 km is the sunspot active region model of Avrett (1981). The model includes energy losses due to Coulomb collisions, removal by nuclear reactions, magnetic mirroring in the convergent flux tube, and MHD pitch-angle scattering in the corona.

Pitch-angle scattering can be characterized by its mean-free-path Λ , the average distance for isotropization. Here Λ is expressed by λ , the ratio of Λ to the loop half-length. With no PAS ($\lambda \rightarrow \infty$), particles with large initial pitch angles mirror and tend to interact at their mirror points where the density is greatest. Particles with pitch angles too small to mirror enter the “loss cone” and either undergo a nuclear reaction as they are moving downward or are thermalized. Without PAS, most particles are moving parallel to the solar surface when they interact (i.e., a “fan beam”). Scattering causes the loss cone to be continuously repopulated and more downward-directed interacting particles. As PAS is increased (λ decreased), the distribution becomes more downward-directed until saturation is reached ($\lambda \sim 20$). At saturation, particles are scattered into the loss cone as quickly as they are removed by interactions so that further decrease of λ has no effect on the temporal or angular dependence of the interactions. Using γ -ray line data from several *SMM* flares, Share et al. (2002) showed that the measured deexcitation-line Doppler shifts imply interacting-ion angular distributions that are inconsistent with no PAS. Better fits were obtained with both nearly-saturated ($\lambda = 300$) and saturated PAS. Figure 10 of Share et al. (2002) shows examples of interacting-particle angular distributions calculated for various values of λ .

Recently, Hua et al. (2002) developed new neutron production kinematics and updated the neutron production cross sections used previously (Hua & Lingenfelter 1987a). We use these cross sections and the loop model to calculate the neutron capture-line time history.

We use a loop length of 1.15×10^9 cm and $\delta = 0.2$, values found by Hua et al. (1989) to provide good fits to deexcitation-line decay times in the 1980 June 21 flare. The ambient medium composition was assumed to be coronal (Reames 1995) but with $\text{Ne/O} = 0.25$ and $\text{He/H} = 0.10$. We assumed “impulsive flare” abundances for the accelerated ions (Ramaty et al. 1996) with an α /proton ratio of 0.5. The accelerated ions are released isotropically at the top of the loop with a power-law energy spectrum and index s (i.e., E^{-s} where E is energy nucleon $^{-1}$) and are followed until they interact or thermalize. The resulting neutrons are followed until they escape, decay, or are captured. The attenuation and direction of the 2.223 MeV γ rays are recorded.

We have calculated neutron capture-line time histories for various assumptions of the accelerated particle spectral index (s), the photospheric ${}^3\text{He/H}$ ratio, and the level of PAS (λ). Figure 1 shows examples of neutron capture-line time histories calculated for instantaneous release of the accelerated particles. The histories were calculated at the 73° heliocentric angle of the 23 July flare and the accelerated-proton spectrum was normalized to 1 proton above 30 MeV. The time histories fall faster with increasing PAS (decreasing λ), increasing ${}^3\text{He/H}$ and harder spectra (smaller s). (Harder spectra tend to produce neutrons deeper in the atmosphere where the higher density shortens the delay.)

We derive predicted neutron capture-line time histories by convolving the time histories calculated for instantaneous release with a neutron-production time history assumed to be given by the nuclear-deexcitation line flux measured for this flare (see §3). This is appropriate because deexcitation γ -ray and neutron production are similarly delayed relative to the accelerated-particle release and the bulk of the production typically occurs less than 10 s after release (Hua et al. 1989, 2002). We use a Monte Carlo technique to estimate the uncertainties of the predicted neutron capture-line time history due to the uncertainties of the measured deexcitation-line time history.

3. Comparison of the *RHESSI* Data with the Calculations

The background-subtracted count spectrum measured by *RHESSI* near the neutron capture-line is shown in Figure 2. The data were fit with a model consisting of a Gaussian profile for the line, a power law for the electron bremsstrahlung and a nuclear deexcitation-line component. These components and the best-fitting total model are also shown in the Figure. Spectra accumulated every 20 seconds were also fit with this model (Share et al. 2003) and the resulting neutron capture-line and 4–7.6 MeV deexcitation-line time histories are shown in Figure 3. For the very-narrow neutron-capture line, the high spectral resolution of the *RHESSI* detectors compensates well for the instrument’s modest effective area. This

is not true for the broader deexcitation lines; the deexcitation-line flux is relatively poorly known which is a dominant source of uncertainty in the ${}^3\text{He}/\text{H}$ ratio derived here (see below).

Figure 1 shows that the accelerated-particle spectral index affects the time history of the neutron capture-line. The most reliable measure of the index for the energy range relevant to the neutron capture-line is the flux ratio of the capture-line and a narrow deexcitation line such as the 4.44 MeV line of ${}^{12}\text{C}$ since this ratio is fairly independent of the ambient and accelerated-particle composition (e.g., Ramaty et al. 1996). For the July 23 flare, the ${}^{12}\text{C}$ line is too weak to provide a useful index measure. Alternatively, the 4–7.6 MeV deexcitation-line band can be used to improve the statistics, but this ratio is much more sensitive to the assumed abundances. Here, we do not determine the spectral index from the data but rather determine what constraints the shape of the neutron capture-line time history alone can place on the ${}^3\text{He}/\text{H}$ ratio and the level of PAS. We assume two spectral indexes (3.5 and 4.5) that represent the range of measured flare accelerated-particle indexes (Ramaty et al. 1996). For each index we vary ${}^3\text{He}/\text{H}$ from 0.1 to 20×10^{-5} and interacting angular distributions due to levels of PAS from none ($\lambda \rightarrow \infty$, a fan beam) to saturated ($\lambda = 20$, strongly downward-directed). We also considered an angular distribution that is 100% downward-beamed. For each combination of index, ${}^3\text{He}/\text{H}$, and angular distribution, a predicted neutron capture-line time history was calculated and compared with the data, normalizing the predicted profile to minimize χ^2 . χ^2 was calculated using uncertainties determined by adding in quadrature the data statistical uncertainties and the estimated prediction uncertainties. Confidence levels for ${}^3\text{He}/\text{H}$ and λ were established assuming two parameters of interest (Lampton et al. 1976).

The minimum χ^2 achieved (χ_{min}^2) was the same for both spectral indexes (60.0 for 44 degrees of freedom, or a confidence level of 5%). Figure 3 shows the measured and best-fit predicted time histories for $s = 4.5$. The dotted lines indicate the time interval for calculating χ^2 (00:28:20–00:43:20 UT). We note that during the rise of the line flux, the prediction exceeds the data for four 20-s intervals by about $2\text{-}\sigma$ each. This could be due to an overestimation of the deexcitation-line flux early in the flare when the flux was weak. Alternatively, the accelerated-particle energy spectrum could have been steeper during this time than during the bulk of the flare, with less neutron production relative to deexcitation-line production. But this would result in a relatively high flux during this time of those deexcitation lines having low cross-section thresholds, such as the 1.634 MeV Ne line, which was not observed.

For each spectral index (3.5 and 4.5), Figure 4 shows how $\Delta\chi^2$ (the change of χ^2 from χ_{min}^2) varies as λ and ${}^3\text{He}/\text{H}$ are varied. (Note: for each value of a given parameter, the other parameter has been adjusted to minimize χ^2 .) For these two indexes, the results for

λ (panel a) do not depend strongly on index. Minimum χ^2 is achieved at $\lambda = 2000$ with a $1\text{-}\sigma$ allowable range of 700–5000 and a 99%-confidence upper-limit of ~ 7000 (assuming two parameters of interest). PAS levels from weak to none can therefore be rejected, implying that the interacting-particle angular distribution must be at least somewhat downward-directed. On the other hand, while more strongly downward-directed distributions ($\lambda < 700$) result in worse fits, even saturated PAS ($\lambda = 20$) cannot be rejected. However, the minimum χ^2 achieved assuming a 100% downward-beamed angular distribution was 68.3, or $\Delta\chi^2 = 8.3$. The downward beam can therefore be rejected with better than 98% confidence.

Smith et al. (2003) find that a 100% downward-beam reproduces the strong deexcitation-line red shifts observed for this flare better than a downward-isotropic distribution, unless the magnetic loop is inclined toward the Earth. Calculations of neutron capture-line production for inclined magnetic fields have not yet been performed. But, longer decay times can reasonably be expected from inclined fields (at least for strong PAS where the interacting angular distribution is more forward directed) since the neutrons would tend to be produced at shallower depths. This may explain why the neutron capture-line analysis favors angular distributions that are less downward-directed than that favored by the narrow-line analysis.

Figure 4 shows that the derived ${}^3\text{He}/\text{H}$ ratio (panel b) depends on the index, with higher values of ${}^3\text{He}/\text{H}$ required for the steeper spectrum (larger s) as expected. The allowable range of ${}^3\text{He}/\text{H}$ ($1\text{-}\sigma$, two parameters of interest) over the range of indexes assumed here was from 0.5 to 10×10^{-5} . If the spectral index were determined by an independent method (e.g., γ -ray line fluence ratios), this allowable range would be reduced. But even so, the ${}^3\text{He}/\text{H}$ uncertainty obtained here would still be significantly larger than those obtained by previous investigators (see §1). In part, this is due to the simultaneous determination of ${}^3\text{He}/\text{H}$ and the interacting angular distribution (λ) which has not been done before. However, we find that most of the uncertainty expressed in Figure 4 arises from the large statistical errors of the nuclear-deexcitation line flux used to represent the neutron-production time history (see Figure 3). Improving the estimate of this time history with better measurements of the nuclear line flux should result in a more constrained ${}^3\text{He}/\text{H}$ ratio estimate.

This work was supported by NASA DPR S13,777G. The work at the UCB and NASA Goddard was supported by NASA contract NAS 5-98033. We thank Benzion Kozlovsky for useful discussions and Hugh Hudson and Brian Dennis for comments on the manuscript.

REFERENCES

- Avrett, C. W. 1981, in *The Physics of Sunspots*, ed. L. E. Cram & J. H. Thomas (Sacramento Peak Observatory:AURA), p. 235
- Chupp, E. L., Forrest D. J., Ryan, J. M., Cherry, M. L., Reppin, C., Kanbach, G., Rieger, E., Pinkau, K., Share, G. H., Kinzer, R. L., Strickman, M. S., Johnson, W. N., & Kurfess, J. D. 1981, *ApJ*, 244, L171
- Hua, X.-M., & Lingenfelter, R. E. 1987a, *Solar Physics*, 107, 351
- Hua, X.-M., & Lingenfelter, R. E. 1987c, *ApJ*, 319, 555
- Hua, X.-M., R. Ramaty & Lingenfelter, R. E. 1989, *ApJ*, 341, 516
- Hua, X.-M., Kozlovsky, B., Lingenfelter, R. E., Ramaty, R. & Stupp, A. 2002, *ApJS*, 140, 563
- Lampton, M., Margon, B., & Bowyer, S. 1976, *ApJ*, 208, 177
- Murphy, R. J., Share, G. H., Grove, J. E., Johnson, W. N., Kinzer, R. L., Kurfess, J. D., Strickman, M. S., & Jung, G. V. 1997, *ApJ*, 490, 883
- Prince, T. A., Ling, J. C., Mahoney, W. A., Riegler, G. R., & Jacobson, A. S. 1982, *ApJ*, 255, L81
- Prince, T. A., Forrest, D. J., Chupp, E. L., Kanbach, G., & Share, G. H. 1983, 18th Internat. Cosmic-Ray Conf. (Bangalore), 4, 79
- Ramaty, R., Mandzhavidze, N., & Kozlovsky, B. 1996, in *High Energy Solar Physics*, ed. R. Ramaty, N. Mandzhavidze, & X.-M. Hua (New York:Am. Inst. Phys.), 374, 172
- Rank, G., Ryan, J., Debrunner, H., McConnell, M., & Schonfelder, V. 2001, *A & A*, 378, 1046
- Reames, D. V. 1995, *Adv. Sp. Res.*, 15, No. 7, 41
- Share, G. H., Murphy, R. J., Kiener, K., & de Sereville, N. 2002, *ApJ*, 573, 464
- Share, G. H., Murphy, R. J., Smith, D. M., Lin, R. P., Shih, A. Y., Hudson, H., Schwartz, R. A., & Kozlovsky, B. this volume
- Smith, D. M., Share, G. H., Murphy, R. J., Schwartz, R. A., Shih, A. Y., & Lin, R. P., this volume

Trottet, G., Vilmer, N., Barat, C., Dezalay, J. P., Talon, R., Sunyaev, R., Kuznetsov, A., & Terekhov, O. 1993, *A&AS*, 97, 337

Wang, H. T., & Ramaty R. 1974, *Sol. Phys.*, 36, 129

Zweibel, E. G., & Haber, D. 1983, *ApJ*, 264, 648

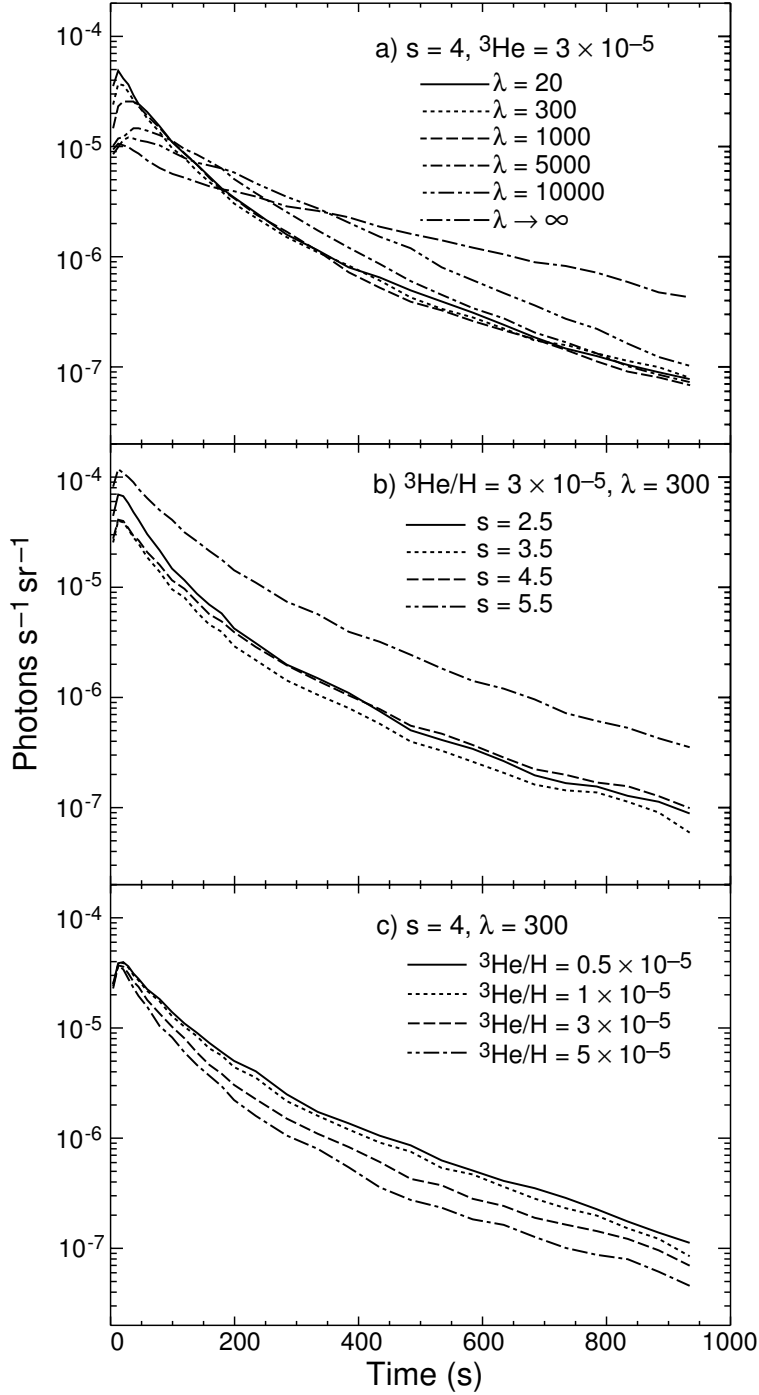


Fig. 1.— Calculations of the neutron capture-line time history showing its dependence on level of PAS (λ), accelerated-particle spectral index (s), and ${}^3\text{He}/\text{H}$ ratio. All calculations are for a loop magnetic field perpendicular to the solar surface at the 73° heliographic angle of the 2002 July 23 flare. The accelerated-particle spectrum is normalized such that there is one proton greater than 30 MeV.

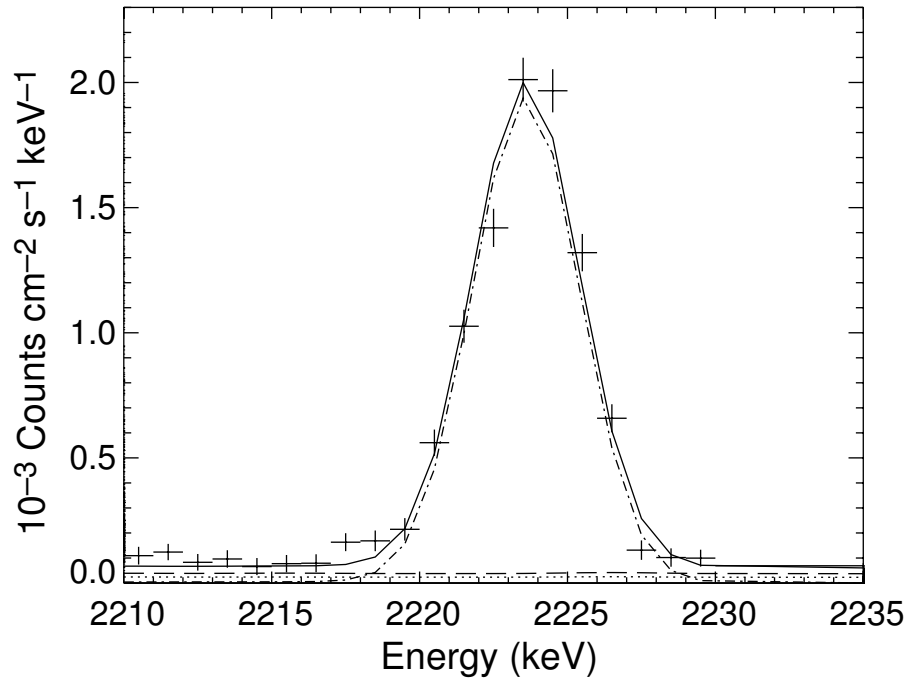


Fig. 2.— The observed 2.223 MeV neutron-capture line count spectrum and the best fit to the data. The dotted curve is the nuclear deexcitation-line component, the dashed curve is the electron bremsstrahlung power law, and the dashed-dotted curve is the Gaussian for the line. The solid curve is the sum of all of the components. The data have been accumulated over the bulk of the flare duration (00:27:20–00:43:20 UT). (Note: above 2230 keV, the data are binned in large energy channels.)

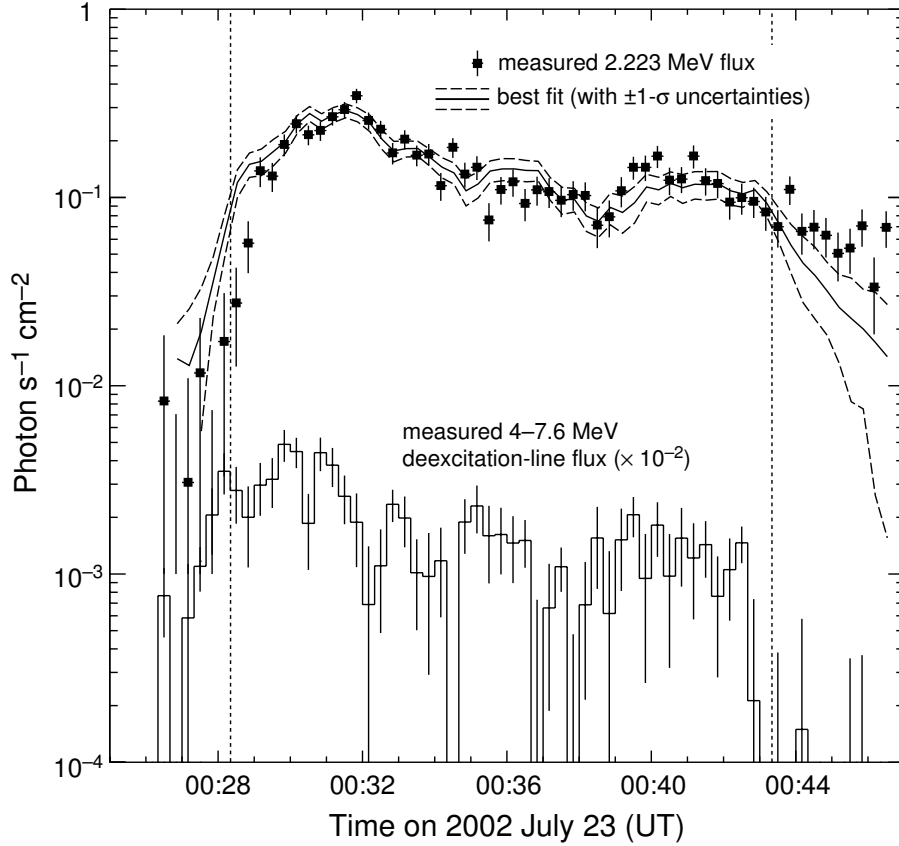


Fig. 3.— Measured time dependences of the 2.223 MeV neutron capture-line and the 4–7.6 MeV deexcitation-line fluxes. The 4–7.6 MeV flux has been reduced by a factor of 100 for clarity. Also shown is the comparison of the best-fitting predicted neutron capture-line flux for $s = 4.5$ (obtained with $\lambda = 2000$ and ${}^3\text{He}/\text{H} = 7 \times 10^{-5}$) and the measured time history. The dotted lines indicate the time interval over which χ^2 was calculated (00:28:20–00:43:20 UT).

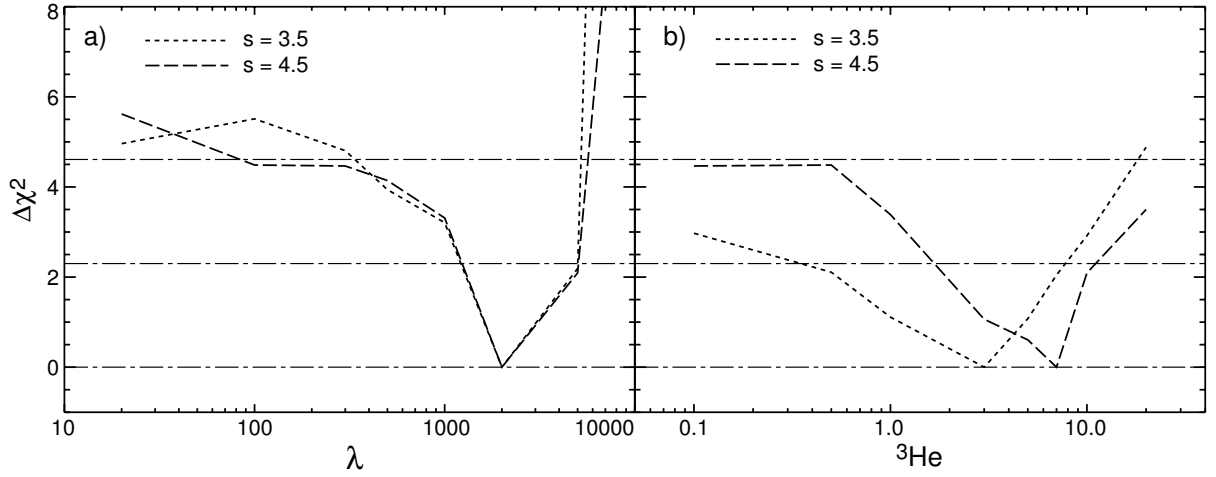


Fig. 4.— Dependence of $\Delta\chi^2 = \chi^2 - \chi_{\min}^2$ for the two parameters λ (panel a) and ${}^3\text{He}/\text{H}$ (panel b) for $s = 3.5$ (dotted) and 4.5 (dashed). The dotted-dashed lines indicate $\Delta\chi^2 = 0$, $\Delta\chi^2 = 2.3$ (68% confidence level for 2 parameters) and $\Delta\chi^2 = 4.61$ (90% confidence level for 2 parameters).